REPORT DOCUMENTATION PAGE

1. REPORT DATE (DD-MM-YYYY) 07-09-2005	2. REPORT TYPE Technical Paper	3. DATES COVERED (From - To)

4. TITLE AND SUBTITLE

Computer Programs for Solar Concentrator Focus Control (POSTPRINT)

5a. CONTRACT NUMBER

5b. GRANT NUMBER

5c. PROGRAM ELEMENT NUMBER

6. AUTHOR(S)

Joseph N. Beasley (AFRL/PRSO); Michael R. Holmes (AFRL/PRSS)

5d. PROJECT NUMBER
1011

5e. TASK NUMBER
0062

5f. WORK UNIT NUMBER

7. PERFORMING ORGANIZATION NAME(S) AND ADDRESS(ES)

Air Force Research Laboratory (AFMC)
AFRL/PRSS
1 Ara Road
Edwards AFB CA 93524-7013

8. PERFORMING ORGANIZATION REPORT NUMBER

AFRL-PR-ED-TP-2005-342

9. SPONSORING / MONITORING AGENCY NAME(S) AND ADDRESS(ES)

Air Force Research Laboratory (AFMC)
AFRL/PRS
5 Pollux Drive
Edwards AFB CA 93524-7048

10. SPONSOR/MONITOR'S ACRONYM(S)

11. SPONSOR/MONITOR'S NUMBER(S)
AFRL-PR-ED-TP-2005-342

12. DISTRIBUTION / AVAILABILITY STATEMENT

Approved for public release; distribution unlimited. PA number: AFRL-ERS-PAS-2005-234.

14. ABSTRACT

   This paper describes two methods for imaging an absorber used as a new sensor in determining the location of the focal spot for a solar concentrator. The absorber is used as a sensor in both methods, but in slightly different ways. The first method developed is an optimization method inspired by Shack-Hartmann wave front sensing. This optimization utilizes masking and a correlation calculation to determine the error from the current image of the focal spot and the ideal or designed position of the focal spot. The second method still uses the absorber as a sensor but calculates area moments of the reflected sunlight on the tubing to calculate the current location of the focal spot.

15. SUBJECT TERMS

16. SECURITY CLASSIFICATION OF:			17. LIMITATION OF ABSTRACT	18. NUMBER OF PAGES	19a. NAME OF RESPONSIBLE PERSON Dr. Michael R. Holmes
a. REPORT Unclassified	b. ABSTRACT Unclassified	c. THIS PAGE Unclassified	A	16	19b. TELEPHONE NUMBER (include area code) (661) 275-5615

Computer Programs for Solar Concentrator Focus Control

Joseph N. Beasley
USAF/AFRL/PRSO
Cal. State University, Long Beach
Claremont Graduate University
8 Draco Drive
Edwards AFB, CA 93524

Michael R. Holmes
USAF/AFRL/PRSS

Abstract:
This paper describes two methods for imaging an absorber used as a new sensor in determining the location of the focal spot for a solar concentrator.The absorber is used as a sensor in both methods, but in slightly different ways. The first method developed is an optimization method inspired by Shack-Hartmann wave front sensing. This optimization utilizes masking and a correlation calculation to determine the error from the current image of the focal spot and the ideal or designed position of the focal spot. The second method still uses the absorber as a sensor but calculates area moments of the reflected sunlight on the tubing to calculate the current location of the focal spot.

Introduction:
Solar Thermal Propulsion (STP) is a unique and promising technique for use in orbital transfers, deep space missions, or other upper stage missions requiring higher specific impulse engines. The main difference between STP and chemical propulsion systems is that STP systems have the energy readily available in space in the form of solar radiation, whereas a chemical propulsion system must carry both propellant and oxidizer into orbit. Since STP doesn't need to carry oxidizer, it will be lighter and easier to carry to orbit than a chemical propulsion system.

Control of the position of the solar concentrators to ensure proper heating of the thruster is paramount in STP. The two concentrators focus and concentrate the light from the Sun onto the absorber, which is actually a portion of the thruster that heats the propellant, usually gaseous Hydrogen which when expanded through a nozzle provides thrust. One other consideration for the control of the concentrators is the requirement to protect the concentrators from the exhaust of the thruster, while maximizing the heat being transferred to the thruster. Prior work settled on an arbitrary control requirement of 0.1 degree in angular position and 0.1 inch in translation[1].

A previous paper[2] presented the idea of using the absorber of the thruster as a sensor for tracking of the focal spot on the absorber. This paper presents two algorithms used in determining the location of the focal spot using the absorber as the primary sensor. Both algorithms utilize concepts developed from studies of the Shack-Hartmann Wavefront sensor. The first algorithm described uses correlation and masking for locating and tracking the focal spot. The second algorithm simplifies the method in algorithm one to using area moments for tracking sunlight.

Results and Discussion:
SYSTEM DESCRIPTION:

Since reference 2 presents the hardware being used for focal spot tracking in detail, a brief summary of the components will now be presented for use in this paper. The schematic of the hardware is shown in Figure EX1 and consists of a CCD camera and a conical shaped

tubular absorber. The new sensor and algorithms are based on the Shack-Hartmann wave front sensor with the holes and lenslets replaced by the cylindrical mirrors of the current system. Sunlight reflecting on the absorber tubing is imaged by the camera for analysis instead of imaging the array of holes or lenslets of the Shack-Hartmann device. The thruster tubes serve as high temperature lenslets. The absorber takes the heat from the sunlight and conducts it to the Hydrogen gas for use in providing thrust. Differences in location of light and how much light is reflected from the tubes are used to determine the focal spot location error for use in a feedback control system.

Two or possibly three different algorithms will be used to locate the focal spot error from the images of the tubes. Different algorithms were deemed necessary because of the 0.1 degree arbitrary control requirement and not having one universal algorithm that covered the three regimes of focus (Sunlight more than 5 diameters off focus), intermediate focus (approximately 5-3 diameters off focus), and fine focus (2-1 diameters off focus).

ALGORITHMS:

METHOD ONE:

The image processing portion of the focus control system was developed along two paths. The first method to be discussed is the more general method using correlation, while the second method is less general based on area moments and area centroids similar to one version of the Shack-Hartmann analysis. The flow chart in Figure XX2A shows the sequence to be implemented for solar concentrator focus control.
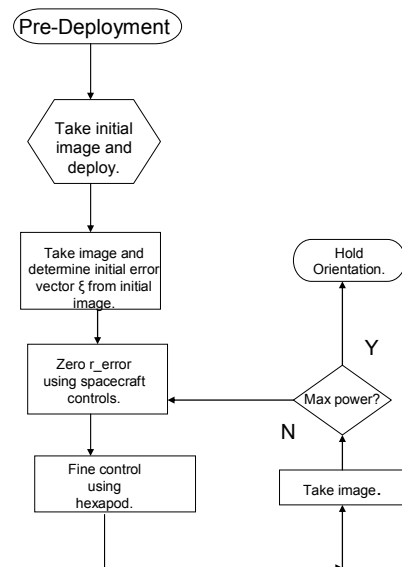

Figure XX2A Flow Chart of Sequence.

Figure XX2 illustrates the diagram for the derivation of the correlation method of focal spot tracking. The method to be described here assumes that the concentrator and camera have been deployed into a configuration that has the concentrator pointing towards the Sun and the camera pointed at the thruster (absorber). The focal spot is located in the general area of the sensor but not on the optimized spot and that the system is not thrusting. Thus, after deployment and coarse alignment, the camera is pointed at the absorber and the concentrator is positioned facing the sun. This situation is then defined as the initial position for the control algorithms. With the addition of a stored image of the absorber in the on-Sun and on-focus designed and geometric configuration, the control algorithms begin.
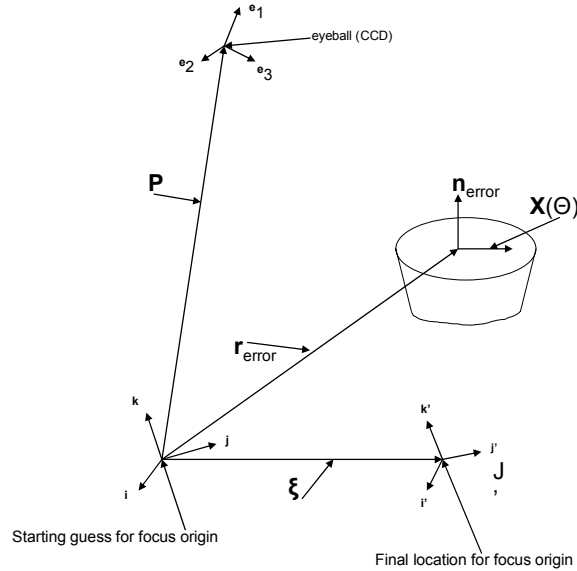
Figure XX2 Starting Coordinates For Correlation

At the start of the control program, the control computer has the initial configuration and initial image in memory. These initial conditions also define an initial coordinate system as displayed in Figure XX2. Also stored in the control computer are masks to be used in computing where the focal spot is currently located each iteration. The correlation or the lack of correlation at the masked areas indicates the current location of the spot and indicates the direction of travel required to reduce the mismatch. The overall process for this control algorithm follows image correlation or scene matching from computer pattern recognition[3]. Both procedures follow a similar mathematical development to that of correlation between masked areas of the test image with the image of the on-focus image. Optimization is utilized to find the optimal and correct focal spot location.

From Figure XX2, $\underline{r}_{error}$, $\underline{p}$, $\underline{X(\theta)}$, and $\underline{n_{error}}$ are the primary vectors in the development of the algorithms. When the system is deployed on orbit, the initial position of the concentrator, camera, and thruster determine the initial origin and coordinate system. $\underline{r}_{error}$ is the vector that determines the location of the image in the original coordinate system for the focus spot. $\underline{n_{error}}$ is the vector normal to the plane at the current image location at $\underline{r}_{error}$. $\underline{p}$, is the location of the camera or "eye-position" with respect to the original coordinate system. Finally, $\underline{X(\theta)}$ is the vector representing areas of the images that are regions of interest to locating the focal spot. The regions of interest in the case of these algorithms would be the thruster itself or the individual rings of the absorber. The required accuracy of focal spot location determines whether the thruster as a whole would be the region of interest or the individual rings.

For the imaging portion of the process, the vector $\underline{X(\theta)}$ in the proceeding paragraph would have to be projected onto the CCD camera image plane. The method used for this operation is based on pinhole optics and perspective projection. The CCD camera utilizes a pinhole aperture for its infinite depth of field. A lens is positioned just behind the pinhole to focus the pinhole image onto the CCD matrix in the camera.   With these optical parameters the projection of $\underline{X(\theta)}$ onto the CCD matrix with coordinates (a,b) is determined using the following equations.

$a(\theta) = \alpha*((\underline{X(\theta)}+ \underline{r}_{error}- \underline{p})\cdot\underline{ehat_1})\diagup(\underline{X(\theta)}+ \underline{r}_{error} – \underline{p})\cdot \underline{ehat_3}$ 　　　　EQN 1

$b(\theta) = \beta**((\underline{X(\theta)}+ \underline{r}_{error}- \underline{p})\cdot e\underline{hat_2})\diagup(\underline{X(\theta)}+ \underline{r}_{error} – \underline{p})\cdot \underline{ehat_3}$ 　　　　EQN 2

α and β in EQN 1 and EQN 2 are scaling factors determined by the CCD pixel size. The **ehat** vectors are unit vectors located at **p** defining a coordinate system at **p** for the camera.

Now that the image and system coordinates and vectors have been defined, the correlation function is derived. The image taken by the CCD will be denoted I(a, b) and is a function of (α, β) as expected. W (α, β) will represent the image or sub-image that we are trying to match. For example, W (α, β) would represent the ideal on-focus image or it could represent only a portion of the ideal image such as specific rings of the sensor. The L_2 norm will then be utilized to calculate the minimum distance between W (α, β) and the current image.

$E(m,n) = \{\sum_{j=1}^{J} \sum_{i=1}^{I} [\, I(i+m-1,j+n-1) - W(I,j)]^2\}^{0.5}$ EQN 3

Where E(m,n) is the measure of distance at coordinates (m,n)

EQN 3 also assumes that W is smaller than the image I, but that does not preclude using a W that is equal to I in size. Square and expand both sides of EQN 3 while using the assumption that the energies in W and I are constant and very small, the correlation of W and E results as shown in EQN 4.

$E^2 (m, n) = -2 \sum_{j=1}^{J} \sum_{i=1}^{I} I(i+m-1,j+n-1)W(I,j)$ EQN 4

Multiplying EQN 4 by -1/2 generates the correlation R(m,n) at (m,n) as shown in EQN 5.

$R(m,n) = \sum_{j=1}^{J} \sum_{i=1}^{I} I(i+m-1,j+n-1)W(I,j)$ EQN 5

Finding the maximum value for R(m,n) will determine the best location in the image that matches W. Finding the X,Y location of the maximum value for R(m,n) and determining the difference from that location to the location of the autocorrelation of the on-focus image determines which direction to move the image to match the maximum correlation. Once the difference between the autocorrelation of the on-focus image location and the point of maximum correlation is found, the control system would move the concentrators to reduce this difference. EQN 5 correlation was thought to be sufficient for determining the location of the focus.

MASKS:

Several different masks were generated to determine which masks to use for determining the focal spot location. Best in this usage means that the masks were best suited to determining the offset distance from the focus location. Several masks that were used with the tubular absorber are shown in Figures XX3, XX4, and XX5. Similar masks were used with the loop of tubing that replaced the absorber for testing. The difference in the masks was which ring of the absorber was used in preparing the mask. For the outer ring mask, the outermost ring of the absorber was used as the masking area and thus enclosed a bigger area of the image than that covered by the inner ring mask. So although the masks in Figures XX3 and XX4 look alike, they, in fact, cover very different regions of the images. The mask in Figure XX5 was thought to be able to isolate a portion of the outer ring for consideration. In actual practice, it matched too many intensity levels to be of use, especially once the light got less than 4 diameters off of focus. In other words, Figure XX5 could not be used to discriminate below about 4 diameters as its correlation was smeared and did not produce impulse-like behavior at correlation.
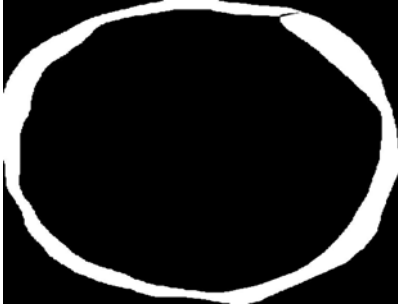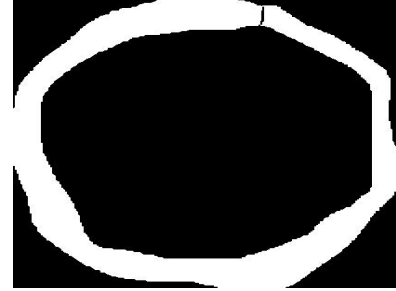
Figure XX3 Outer Ring Mask

Figure XX4 An Inner Ring Mask

Figure XX5 "Banana" Shaped Mask

METHOD TWO:

The second method for determining focal spot location is by measuring light area moments in the image. This method is derived based on a modification of the Shack-Hartmann wave front sensor using cylindrical mirrors instead of lenslets to register light areas[4]. Images of the concentrator can be seen in each coil of the absorber. Whether a particular image on the tube, denoted as a "tube blob" is bright or dim depends on how close the tube is to the focal point. Image area moments are then used to quantify focus for individual "tube blobs." The derivation also follows from a discussion of area moments and centroids from mechanics[5]. An image is acquired via the CCD camera and a threshold is applied to the image for further processing.

Typical Image

Tube "Blob"

Tube

Tube "Blob"

Plate
"Blob"

Tube "Blobs" can appear anywhere
along or on the tube.

Plate "Blobs" appear on the plate
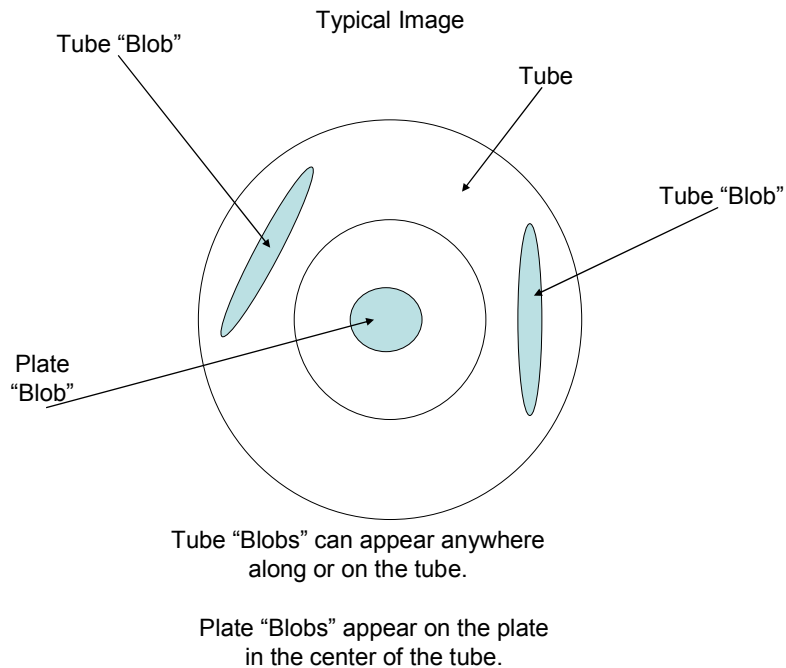in the center of the tube.

Figure AM1 Generic Light Patterns in Image of tube in the Sensor.

Figure AM1 shows a generic schematic of light blobs from an image of the sensor. As explained earlier, each tube "blob" is an actual image of the light from the concentrator. The shape and intensity area of each tube blob is related to the amount of light in the concentrator being concentrated to that area of the tube. Calculating the area centroid of the images in the tubes determines where the focal spot is located on this iteration of the algorithm and knowing where the centroid of the focal spot is located for this iteration determines which direction the control algorithm needs to move the concentrator to move the centroid to the center of the sensor.
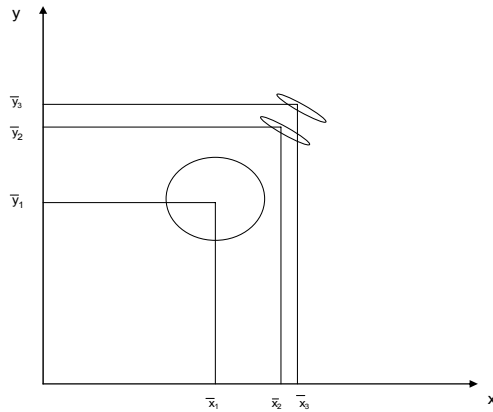
Figure AM2 Light in Image From CCD.

Figure AM2 shows the situation that might occur once the CCD acquires an image. A coordinate system for the image is setup as shown in Figure AM2. The image is then processed by first thresholding the image and then calculating the area moments for each light area. The threshold is set, at least in the ground experiments, by visually making sure that the lighted areas in the sensor tubes do not overlap into the area of the secondary concentrator. On flight another method of preventing overlap would be needed, possibly a measured area of the absorber beyond which the controller would ignore. Once the image has been thresholded, the area moments are calculated and an average or overall centroid is calculated as the location of the focal spot on the sensor.
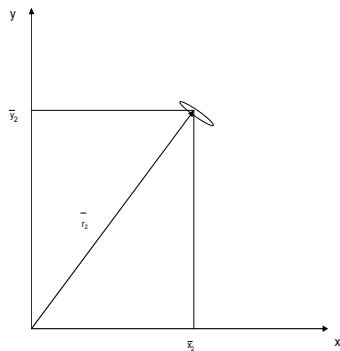

Figure AM3 Calculation Schematic.

Figure AM3 is an ideal schematic of the calculation for one of the ellipse shaped light areas. The light area is located at **r₂** and the area calculated as (π*a*b)/4, where (a) is the major axis of the ellipse and (b) is the minor axis of the ellipse. Position vector **r₂** is the vector from the origin to the center of the ellipse.
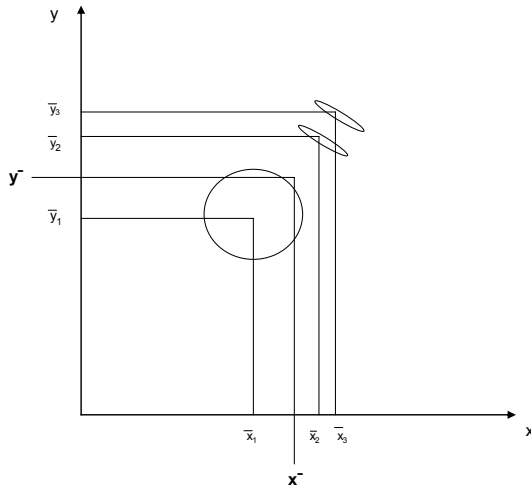

Figure AM4 Centroid Calculation.

Finally, Figure AM4 shows the calculations shown in Figures AM2 and AM3 combined to calculate the overall area centroid. As shown in Figure AM4, the image of the central flat plate will have a significant "blob" of light located at the center of the sensor as the control described in this paper assumes a coarse focus is obtained before the methods of this paper are used for fine focus. If the "blob" of light in the center of the image is too big for the area centroids to be calculated, it can be suppressed in the calculation of centroids to obtain locations that are very close to focus.

EXPERIMENTAL SETUP:

Figure EX1 depicts the setup used for collecting images for analysis. The source of light used was a 3 inch diameter red LED taillight. The size of the light gives an extended source a little over half of the Sun's diameter as viewed from the concentrator. For the setup shown in figure EX1, the size of light that corresponds to Earth's orbit is approximately 5 inches in diameter. SRS Technology's 1X2 meter elliptical concentrator was used to focus light on the thruster/absorber and secondary concentrator as well as the later imaging of the single loop of tubing utilized in the study of misalignments closer than 2-3 diameters off of focus.

Images were obtained using a STX-10XE CCD camera from Santa Barbara Instrument Group (SBIG). This camera provides a 2184X1472 pixel 6.8μ CCD for imaging. CCDOPS from SBIG was used on a notebook computer to acquire images at 0.5 sec exposure times. The Sun simulator was connected to a tripod which allowed the Sun simulator to move around at the second focal spot of the concentrator providing the misalignment of the Sun and the concentrator for study. Images were then taken with the Sun simulator at various locations from focus in 1 diameter increments. The maximum distances that were obtainable in the physical layout shown in Figure EX1 was 3-4 diameters off of focus in the X direction and 2-3 diameters in the Z

direction. Movement in the y direction was not checked in these experiments. Figure EX2 and Figure EX3 show the actual equipment used in the experiments. The assigned coordinate axes for the light source are shown in Figure EX4 and in Figure EX5 for the thruster in these experiments. These coordinate systems become more important for control of the hexapod used for moving the concentrator.

Test Apparatus

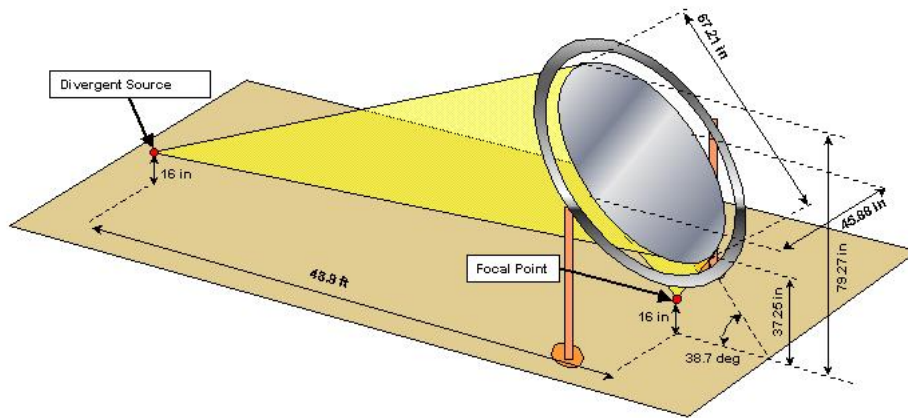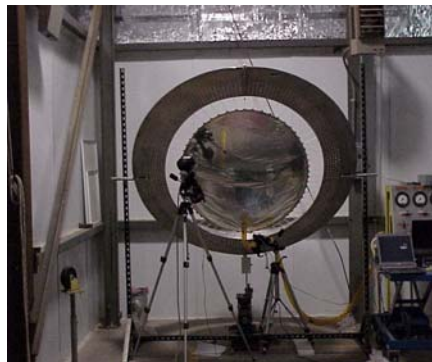

Figure EX1Test Setup.

Figure EX2 Concentrator From Source End.
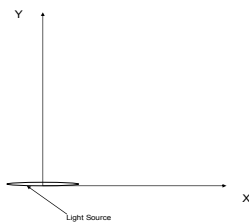
Figure EX3 Divergent Source.

Figure EX4 Top View Coordinate Axes at Light Source For Understanding File Names in Table 1.
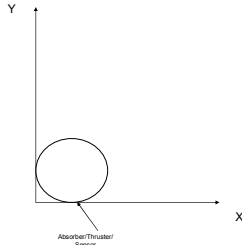

Figure EX5 Top View Coordinate Axes at Thruster For Completeness and Future Work.

IMAGEJ AND IMAGE ANALYSIS[6]

 The ImageJ image analysis and processing package from the National Institutes of Health was used to process the images taken in the experiments. The program provides a Graphical User Interface (GUI) and extensive image analysis commands. ImageJ is also extendable by using either macros or ImageJ plugins. Plugins are basically Java classes that implement one of several interfaces in ImageJ or they are Java classes performing specific operations within ImageJ.

METHOD 1

 ImageJ performs correlation on images using the conjugate multiplication of the Fourier transforms of two images to be correlated. Masks were utilized to reduce the size of images to include only the absorber area as the region of interest. Masking also helped the processing time required for the calculation of the FFTs as the images were reduced from 2184X1472 down to a

more manageable 512X512 while still maintaining the correct region of interest. Results from the processing of various offsets from on-focus are presented in Figures AX1 through AXX.

Figure AX1 shows the autocorrelation result for the on-focus image. It has a very clear "dot" or impulse at the center of the image. This result was expected as the autocorrelation of an image with itself would be an impulse at offset (0,0).

Figure AX2 shows the result for the cross-correlation between the images for up 1 diameter from on-focus of the solar simulator and the on-focus. In this instance, the correlation is smeared and basically located at the center of the image indicating that the 1 diameter misalignment has not been resolved from the on-focus situation in which the maximum value is located in the center of the image.

Figure AX3 shows a much better situation for the correlation technique. This figure shows the correlation between a 4 diameter image and the on-focus image. This figure also shows the result for a mask similar to the one shown in Figure XX5.   The mask used in Figure AX3 has other problems at a smaller offset as the numbers of correlations that may occur in the image get larger as the focus spot gets closer to the on-focus location.
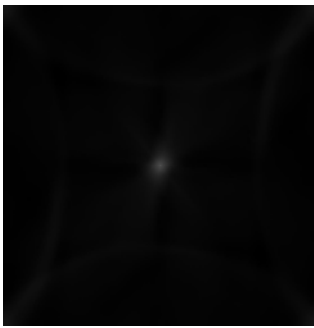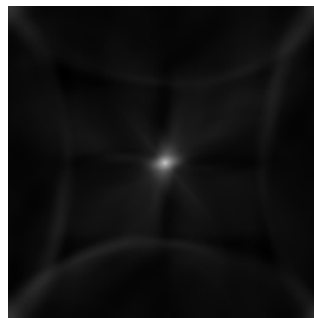

Figure AX1 Autocorrelation

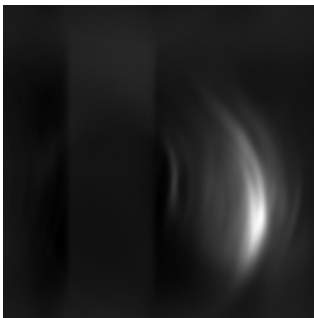Figure AX2 Correlation Up 1 Diameter.

Figure AX3 Correlation 4 Diameter Offset

Figure AX4 Correlation 2 Diameter Offset.

.

The correlation shown in Figure AX4 illustrates the problems involved when using the correlation function at offsets below about 3 diameters. The correlation in Figure AX4 shows that an offset exists; however, the offset itself cannot be determined from this image. The cutoff for using masks like those in Figures XX3 and XX4 using correlation defined by EQN 5 appears to be between 2 and 3 diameters of offset.

However, at this point it was noted that using only EQN 5 lead to problems as it would find any and all correlations based on the maximum intensities present, with little regard for the variations in intensities present in an area of the image, instead of the correct correlation value. That is, EQN 5 would pick an area in I(m,n) that in general had very high intensities instead of actually the point of highest correlation. That problem is eliminated by dividing EQN 5 by the total energy in I(m,n), $(\sum_{j=1}^{J} \sum_{i=1}^{I} I^2(i+m-1,j+n-1))^{0.5}$.   Furthermore, EQN 5 can be normalized to the range (-1,1) by dividing by the energy in W(m,n). It was not necessary to divide by the energy of

W(m,n) for the case being discussed in this paper as it was not important to get values from (-1, 1). Another form for EQN 5 is known as the phase only correlation that basically divides W(m,n) by the magnitude of W(m,n), which normalizes the FFT of W providing only the phase information which provides a more impulse-like function for the correlation. As a quick approximation of the phase only correlation, a high pass filtering was tried since the phase only EQN is similar to EQN 5 but with the addition of dividing by the magnitude of W. Dividing by the magnitude of W, with W having low pass frequency patterns, is approximately high pass. The result shown in Figure AX1 shows one application of the high pass filtering for the autocorrelation. The phase only correlation will be looked at in a future paper.

METHOD 2

ImageJ was also utilized for the analysis outlined in method two of this paper. The particular command used was the "Analyze Particles" of the Analyze menu. To prepare the images for analysis, each image had to have a threshold applied before "Analyze Particles" would work. For the experiments in this paper the automatic threshold was used for all images. It was felt that auto threshold would be fine for verifying the concepts and algorithms presented in this paper. Table one lists the various particles found in calculating the areas and centroids for each image examined. Particle analysis does not require masking so no masks are indicated. The label column describes the image file which also presents the source positioning information for that image. For example the label "up0diam_1diam_pos_x…" indicates that the source light was positioned 1 diameter off of center in the positive X direction and was not moved vertically, etc. Figures EX4 and EX5 present the corresponding coordinate axes for both the source and the thruster as used in Table 1.

	Label	Area	X	Y	Major	Minor	Angle
1	on_focus_pt5secs_4_aug_2005	4343	276.746	29.401	182.604	30.282	166.102
2	on_focus_pt5secs_4_aug_2005	16891	292.18	139.54	160.747	133.908	134.72
3	on_focus_pt5secs_4_aug_2005	1175	304.546	429.943	109.479	13.665	14.483
4	up0diam_1diam_pos_x_pt5secs_4_aug_2005	6187	185.416	35.906	183.007	43.066	11.87
5	up0diam_1diam_pos_x_pt5secs_4_aug_2005	27247	258.621	161.973	218.615	158.964	120.044
6	up0diam_1diam_pos_x_pt5secs_4_aug_2005	2705	203.531	424.335	166.181	20.733	164.91
7	up0diam_1diam_neg_x_pt5secs_4_aug_2005	3978	337.551	55.936	173.186	29.253	147.823
8	up0diam_1pt5inch_neg_x_pt5secs_4_aug_2005	5127	314.891	44.521	189.146	34.519	154.33
9	up0diam_1pt5inch_neg_x_pt5secs_4_aug_2005	6695	334.321	130.899	117.068	72.848	133.903
10	up0diam_1pt5inch_pos_x_pt5secs_4_aug_2005	5195	178.505	38.044	168.821	39.188	13.164
11	up0diam_1pt5inch_pos_x_pt5secs_4_aug_2005	28812	253.873	178.983	225.809	162.904	116.247
12	up0diam_1pt5inch_pos_x_pt5secs_4_aug_2005	3686	187.472	418.152	188.46	24.916	161.517
13	up0diam_2diam_neg_x_pt5secs_4_aug_2005	4431	375.153	86.678	182.028	30.994	135.517
14	up0diam_3diam_neg_x_pt5secs_4_aug_2005	4091	383.473	93.188	175.383	29.7	133.809
15	up0diam_2diam_pos_x_pt5secs_4_aug_2005	280	182.303	10.264	30.403	11.894	13.253
16	up0diam_2diam_pos_x_pt5secs_4_aug_2005	3431	69.194	94.311	150.213	29.099	52.783
17	up0diam_2diam_pos_x_pt5secs_4_aug_2005	22244	203.33	195.177	224.069	127.143	121.013
18	up0diam_2diam_pos_x_pt5secs_4_aug_2005	5181	86.968	354.649	210.627	31.325	138.272
19	up0diam_3diam_pos_x_pt5secs_4_aug_2005	1447	45.048	126.181	78.912	23.347	65.158

| 20 | up0diam_3diam_pos_x_pt5secs_4_aug_2005 | 2634 | 28.036 | 295.441 | 139.366 | 24.064 | 119.143 |
| 21 | up0diam_3diam_pos_x_pt5secs_4_aug_2005 | 211 | 176.264 | 252.713 | 24.213 | 11.358 | 113.949 |

Table 1 Images and Area Calculations with Centroids and Ellipse parameters.

The columns in Table 1 for major, minor and angle are the parameters for ellipses that approximate the areas of light in the images. These parameters were taken for future analyses that involve using the major axis and minor axis values to determine shrinkage or elongation of the light areas that may be useful to increase the effectiveness of the area moment method for determining focal spot location. The angle parameter is related to the angle between the major axis of each ellipse and a line parallel to the horizontal or X axis in the image. The angle and the length measurements could be combined into the method of area moments to enhance the focal spot location determination.

Figure AX5 On-focus Image for Area Measurements.

Figure AX5 presents the situation in the process after the image has been cropped and a threshold has been applied. The next step in the process is shown in figure AX6 when ImageJ has calculated the individual areas based on a minimum size of 100 pixels. The 100 pixel limit came from an approximate value of 2000 pixels that would be in a "tube blob" area calculation for a fully lit concentrator on-focus. The 100 pixel area represented 3-5% of full light, so that we looked for light areas representing 95% fully illuminated concentrator. The values for the centroids and areas for the image shown in Figure AX6 are shown in table 1 with label on_focus_pt5secs_4_aug_2005. Calculations for the image: up0diam_1diam_pos_x_pt5secs_4_aug_2005 gave an average X value of 194.473 and average Y value of 230.12. The method then uses either the centroid of the central "plate blob" of light or the centroid of the on-focus image to generate the difference signal used for concentrator control.

For the "tube blob" analysis, the difference calculation gives a |X| difference of 64.148 and a |Y| difference of 68.147. By subtracting the focal spot centroids from the centroid of the "blob" a direction of movement towards focus is generated. If the on-focus X and Y centroids are retained from that image a larger displacement value may be generated for the control values that move the focal spot towards focus. When there is no central "plate blob" of light in the image, the centroids for X and Y from the on-focus image have to be used for delta calculations. These delta calculations would then be used to generate control values for the hexapod controller. Looking at table 1, it can be seen that this method works down to at least 1.5 inches off of focus for the solar simulator. That number is associated with 0.15 degrees of offset, which is very close to the requirement that we control to 0.1 degree.
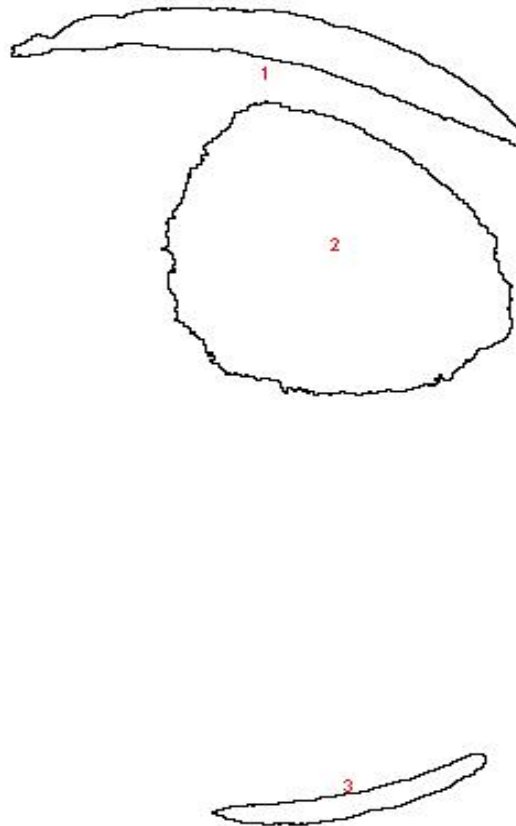

Figure AX6 Resulting Particles Measured From AX5, Blobs 1 and 3 are Concentrator Images on the tube.

SUMMARY AND CONCLUSIONS:

Both methods work for locating the focal spot on the sensor. Correlation using only EQN 5 fails to work below 2-3 diameters of misalignment. Test images using high pass filtering to approximation phase only correlation was begun. This method was not fully implemented for this paper.

Area moments did better below 2-3 diameters of misalignment. Table 1 shows the complete calculations for several images used in this study. Good focal spot tracking was seen

from 5 diameters of misalignment down to 1.5 INCH of misalignment. The 1.5 inch gives about 0.15 degree of misalignment, which is very close to our original requirement.

FUTURE WORK:

Future work will include automating, using ImageJ, the steps outlined in this paper to control either a model of the concentrator and thruster or an actual concentrator with hexapod and thruster. Another area for future work is modifying ImageJ's FFT Math process to implement the phase-only correlation to improve the correlation algorithm to operate with the source light below 2-3 diameters off of focus. Also, a combination of both methods should be studied to overcome the limitations of the correlation method. Finally, data should be taken below 1.5 inches of misalignment to verify that the method can get to the .1 degree of misalignment and improve the control down to 0.02 degrees of misalignment where the thruster acceleration could be utilized in the optimization of concentrator location using a combination of Phase Only Correlation (POC) and area moments or a refined area moment method.

[1] Wassom, Dr. Steven R., "Focus Control System for Solar Thermal Propulsion," 2000 International ADAMS User Conference.

[2] Beasley, Joseph N., "A Novel Wave Front Method Used for Tracking Terrestrial Concentrator Focal Spot Location," 2004 JANNAF Conference.

[3] Wong, Robert Y., Computer Pattern Classification and Scene Matching., The Faculty Press, California State University, Northridge, CA, 1981.

[4] Tokovinin Andrei A., "Tutorial on Adaptive Optics at CTIO", http://www.ctio.noao.edu/~atokovin/tutorial/index.html , Cerro Tololo Inter-American Observatory, July 10,2001.

[5] Hibbeler, R. C, Engineering mechanics, statics. Macmillan Publishing Co., INC, New York, New York, 1978.

[6] Rasband, W. S., ImageJ, U. S. National Institutes of Health, Bethesda, Maryland, USA, http://rsb.info.nih.gov/ij/, 1997-2005.